Measurement of the absolute yield of $CO(a\ ^3\Pi)+O$ products in the dissociative recombination of CO_2^+ ions with electrons

Miroslaw P. Skrzypkowski, Theodosia Gougousi,[a] and Rainer Johnsen
Department of Physics and Astronomy, University of Pittsburgh, Pittsburgh, Pennsylvania 15260

Michael F. Golde
Department of Chemistry, University of Pittsburgh, Pittsburgh, Pennsylvania 15260

(Received 23 January 1998; accepted 20 February 1998)

A flowing-afterglow technique is described for measuring the absolute yield of a radiative product state from ion–electron recombination. The technique is applied to $CO_2^+ + e^-$ dissociative recombination. The measured yield of $CO(a\ ^3\Pi)+O(^3P)$ is 0.29 ± 0.10. This includes cascade from higher triplet states of CO. The vibrational distribution in $CO(a\ ^3\Pi, v=0-3)$ is approximately Boltzmann, with an effective temperature of 4200 ± 300 K. The measured rate constant for quenching of $CO(a)$ by CO_2 is $(1.0\pm0.2)\times10^{-11}$ cm^3 s^{-1}, somewhat lower than previous measurements. © *1998 American Institute of Physics.* [S0021-9606(98)03020-7]

I. INTRODUCTION

Gas-phase recombination of cations and electrons is important in many energy-rich systems such as planetary ionospheres, laser plasmas and in plasma-induced vapor deposition on surfaces.[1–5] For molecular ions, the measured neutralization rate coefficients are extremely large, often of the order of 10^{-7} or 10^{-6} cm^3 molecule^{-1} s^{-1}. Much less is known about the products of this process, but dissociation of the energy-rich neutral intermediate is expected.[6–8] Initial data have recently been obtained, using laser-induced fluorescence,[9,10] emission spectroscopy,[11,12] and kinetic energy analysis[13,14] to identify the resulting fragments and, in suitable cases, to measure their absolute yields.

Light emission from electronically excited fragments is of particular interest because it can, in principle, be applied to remote sensing of the parent ion in practical environments. The dissociative recombination of CO_2^+ ions

$$CO_2^+ + e^- \rightarrow CO + O(^3P, ^1D, ^1S) \tag{1}$$

can give rise to a range of excited states of CO, including $a\ ^3\Pi$, $v<12$, $a'\ ^3\Sigma^+$, $v<11$, $d\ ^3\Delta$, $v<6$, $e\ ^3\Sigma^-$, $v<3$, $A\ ^1\Pi$, $v<2$, and $I\ ^1\Sigma^-$, $v<2$, these limits applying to recombination of the $^2\Pi_{3/2}$ ground state of CO_2^+ with formation of $O(^3P)$. Figure 1 shows potential-energy curves for relevant electronic states of CO. Emission from CO_2^+ dissociative recombination has been observed from both singlet and triplet states of CO. From a study of $CO(A\ ^1\Pi - X\ ^1\Sigma^+)$ uv emission, Gutchek and Zipf[16] deduced a branching fraction of 0.05 for $CO(A\ ^1\Pi)$ formation. Wauchop and Broida[17] and Taieb and Broida[18] studied $CO(a\ ^3\Pi - X\ ^1\Sigma^+)$ emission from discharged $He+CO_2$ in a flowing afterglow. Taking account of the long radiative lifetime,[19,20] 7.5 ms, of $CO(a\ ^3\Pi)$, they deduced a branching fraction of 0.55 for $CO(a\ ^3\Pi)$ formation. They also reported emission from a few vibrational levels of the $a'\ ^3\Sigma^+$, $d\ ^3\Delta$, and $e\ ^3\Sigma^-$ states but the extremely small branching fractions which they derived for these states, 0.008 for $d\ ^3\Delta$ and 4×10^{-4} for $a'\ ^3\Sigma^+$, are probably not reliable, being based on an incomplete spectrum.[17]

Different conclusions were reached in a recent emission study by Tsuji *et al.*[21] of the reactions of CO_2 in a He afterglow. They report relative intensities of emission from all the above-mentioned states. The a' and d states were the strongest emitters and they conclude that the yield of $A\ ^1\Pi$ is smaller than 0.0033. Only about 1% of $CO(a)$ emitted within their observation region. However, they estimated the relative formation rate of this state and concluded that it is populated principally by $a'\rightarrow a$ and $d\rightarrow a$ cascade emission. The implication of their conclusions is that, of these five excited states, only two, the d and a', states are populated initially to an appreciable extent.

In the present study, we have measured the absolute branching fraction for $CO(a\ ^3\Pi)$ formation in the $CO_2^+ + e^-$ reaction and have obtained a value which is comparable to, but smaller than, that of Wauchop and Broida. This value is the sum of direct formation of the $CO(a)$ state and contributions from cascade from the higher triplet states.

The experimental procedure was similar to that adopted in our recent LIF study[10] of the absolute OH yield from the dissociative recombination of H_3O^+ ions. We determined the absolute intensity of $CO(a\ ^3\Pi)$ emission produced by the recombination of a known concentration (or flux) of CO_2^+ ions by means of a calibration technique utilizing reactions with a known branching fraction into emitting states. Two sequences were examined.

Firstly, the well-characterized Penning ionization reaction of $He^*(2\ ^3S)$ metastable atoms with N_2

$$He^* + N_2 \rightarrow N_2^+(B\ ^2\Sigma_u^+) + He + e^- \tag{2a}$$

$$\rightarrow N_2^+(X\ ^2\Sigma_g^+,\ A^2\Pi_u) + He + e^- \tag{2b}$$

[a]Current address: Institute of Electronic Structure and Laser (IESL), Foundation for Research and Technology-Hellas (FORTH), Heraklion 71110 Greece.

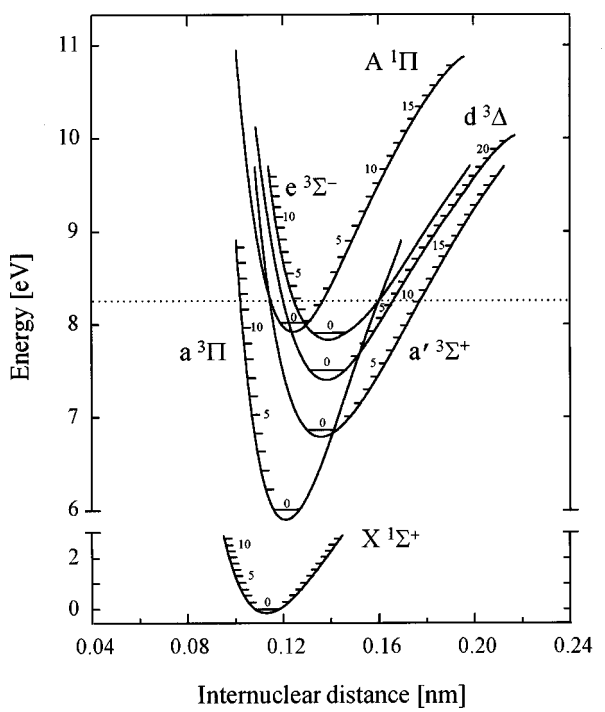

FIG. 1. Potential energy curves of CO, adapted from Ref. 15. The dotted line indicates the maximum internal energy available to CO from dissociative recombination of ground state $CO_2^+ + e^-$.

was used, which has a branching fraction[22] for channel (2a) of 0.41 ± 0.04. The procedure was to monitor the electron density using a Langmuir probe, and the $N_2^+(B-X)$ emission signal.

In the second calibration method, two reactions of $Ar^*(^3P_2)$ metastable atoms were monitored

$$Ar^* + NO \rightarrow Ar + NO^+ + e^- \tag{3}$$

for which the branching fraction[23,24] is 0.35 ± 0.10; and

$$Ar^* + N_2 \rightarrow Ar + N_2(C\ ^3\Pi_u) \tag{4}$$

for which the branching fraction[25,26] is 0.80 ± 0.20. Electron-density measurements for reaction (3) yielded the flux of Ar* metastables. The $N_2(C-B)$ emission signal then provided the absolute calibration of the photon detection system.

Although the $He^* + N_2$ approach appears to be more direct, the data analysis was somewhat more involved than for the second sequence and the calibration somewhat less precise. We therefore preferred the latter route. However, results obtained using the $He^* + N_2$ calibration reaction proved to be consistent, within the experimental error limits, with those obtained from the preferred sequence.

II. EXPERIMENT

The flowing afterglow system has been described fully elsewhere.[10] For this experiment, two separate discharge regions, upstream of the entrance to the 3 cm radius, stainless-steel flow tube, were used. Pure He was passed through a microwave discharge. The resulting mix of He* metastables and He^+ ions was converted, by Ar addition, to an Ar^+/e^- plasma. CO_2 was added downstream through a movable injector to convert Ar^+ rapidly to CO_2^+ ions. For the $He^* + N_2$ experiments, an analogous technique was employed, except that no Ar was added.

For the studies of the $Ar^* + N_2$ and NO reactions, pure Ar was passed through a dc discharge. The reagent was added, as before, through the movable injector. In order to maximize the Ar* density, He gas was added downstream of the discharge. In all experiments, the total gas pressure was between 0.8 and 1.1 Torr and the mean flow velocity was approximately 2500 cm/s. The mole fraction of Ar was about 0.15 in the $CO_2^+ + e^-$ system and about 0.6 in the $Ar^* + N_2$,NO studies. He*, Ar*, and Ar^+ concentrations were in the range: 1×10^9 to 5×10^{10} cm^{-3}. The concentrations of the stable reagents were 10^{12} to 5×10^{14} cm^{-3}.

The electron density along the flow tube was measured by a movable Langmuir probe. In general, this was positioned on the tube axis; however, it could be rotated to measure the density off-axis. The operation of the Langmuir probe has been described previously;[27] it yields absolute local concentrations of electrons.

Emission was collected in a direction perpendicular to the tube axis through a quartz window, which extends most of the length of the flow tube. An assembly consisting of a baffled collimator (which included a collimating lens), 0.2 m monochromator (Acton VM-502) and uv-sensitive photomultiplier (EMI 9789Q) was moved along a rail to collect emission as a function of position along the tube (z direction). The field of view of the detection system was approximately a rectangle, 0.4 cm width (along the z direction) and 1 cm high at the center of the flow tube. The monochromator slit width was 150 μm for all experiments: this corresponds to a spectral resolution of 0.6 nm. The photomultiplier was used in a pulse-counting mode and the output signal was processed by a lab computer. The spectral response of the detection system was measured between 200 and 400 nm using a calibrated D_2 lamp.

The principal measurements are of the electron density and the emission signal as a function of z. It was considered critical to understand the observed behavior in terms of the chemical reactions involved and diffusion (radial and axial) of all species. As described previously,[10] the continuity equation, including diffusion, was solved numerically over a grid with a step size of 1 mm in both the radial and axial directions. The chemistry was initiated by ''addition'' of CO_2 reagent at a single z value. To represent the loop injector, the addition was limited to a ring-shaped region of suitable radius and thickness. The reagent spread radially by diffusion only: no ''jetting'' was incorporated into the simulation. For typical flow conditions, the simulations showed that appreciable radial mixing (with concentration on axis equal to about one-half of the reagent concentration for complete mixing) was achieved 2–3 cm downstream of the loop. The interference to the carrier gas flow caused by the injector loop was also ignored. The following chemical processes were included:

$$Ar^+ + CO_2 \rightarrow CO_2^+ + Ar,$$

$$k_1 = (6.0 \pm 1.5) \times 10^{-10}\ cm^3\ s^{-1} \quad \text{(Refs. 28, 29)}, \tag{5}$$

$$CO_2^+ + e^- \rightarrow CO(a) + O, \quad k_{2a}$$
$$\rightarrow \text{other products}, \quad k_{2b}, \tag{6}$$
$$\text{with } k_2 = k_{2a} + k_{2b} = (3.0 \pm 0.5) \times 10^{-7} \text{ cm}^3 \text{ s}^{-1}$$
$$\text{(Refs. 30, 31)},$$
$$CO(a) \rightarrow CO(X) + h\nu, \quad k_3 = 133 \pm 18 \text{ s}^{-1}$$
$$\text{(Refs. 19, 20)}, \tag{7}$$
$$CO(a) + CO_2 \rightarrow \text{products}, \quad k_4. \tag{8}$$

Quenching of the long-lived $CO(a)$ state by Ar and He is very slow[32] and could be neglected. However, quenching by CO_2, process (8), is significant. Previous measurements[32] have given a range of values of k_4 from 1.2 to 4.1 $\times 10^{-11}$ cm^3 s^{-1}, with a ''recommended'' value of 1.7 $\times 10^{-11}$. The values of k_1, k_2, and k_4 were varied in the simulations to obtain the best fits to the observed z dependences of the electron densities and of the $CO(a-X)$ emission intensity. The simulations also required input of diffusion coefficients for the relevant species. Published values[33–35] of diffusion coefficients (in He and Ar buffer gas) for Ar^+, CO_2, and CO_2^+ were used. An experimental value for $CO(a)$ in He is also available.[35] For $CO(a)$ in Ar, the diffusion coefficient was estimated by analogy with $N_2(A\ ^3\Sigma_u^+)$ in Ar and $Cl(^2P)$ in Ar (Refs. 36, 37); the effective diffusion coefficient of $CO(a)$ was varied in the simulations. The simulations were carried out with $k_{2a} = k_2$. Comparison of the results with the measured emission intensity yielded the branching fraction for $CO(a)$ formation.

High-purity He (99.997%) and Ar (99.998%) were purified further by passage through cold traps in the gas handling system. CO_2 (99.8%) and N_2 (99.998%) were used without purification. NO was purified by passing it through a soda lime trap, as described previously.[10]

III. RESULTS

A. CO($a-X$) emission from recombination of CO_2^+

When CO_2 was added to a stream of Ar^+ ions and electrons, $CO(a-X)$ emission was observed in the region of the reagent inlet and extending more than 10 cm downstream. A typical spectrum measured 4 cm downstream of the inlet is shown in Fig. 2. All features could be assigned to transitions from $CO(a,v=0-4)$; the absence of emission from electronically excited CO^+ and CO_2^+ indicates[38] that essentially no He^+ ions or He* metastables remain in the flow at the point where the CO_2 is added. To verify that the emission does indeed arise from dissociative recombination, traces of SF_6, an efficient electron-scavenger,[39] were added with the CO_2. In the concentration range $[SF_6]=1-3\times10^{12}$ cm^{-3}, the $CO(a-X)$ intensity 1 cm downstream of the injection point was reduced by approximately 90%. Part of this small remaining signal is due to reaction of $Ar(^3P)$ metastables in the flow, at approximately 10% of the Ar^+ concentration:[40]

$$Ar^*(^3P) + CO_2 \rightarrow Ar + CO(a\ ^3\Pi) + O, \tag{9}$$

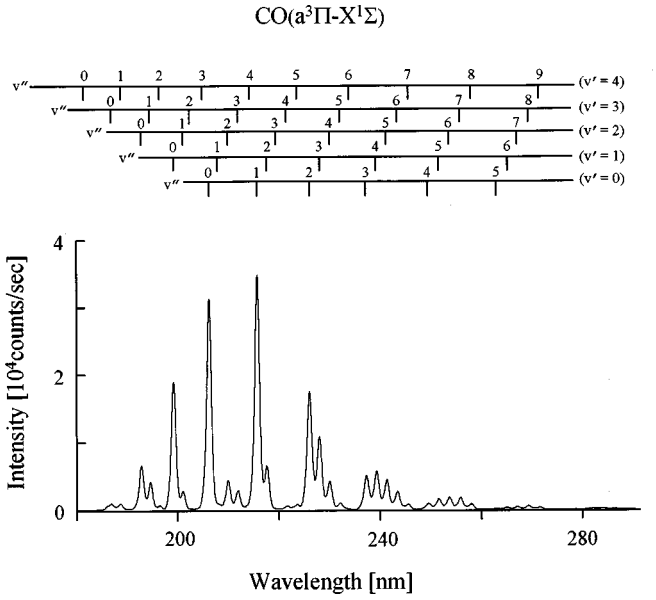

FIG. 2. $CO(a\ ^3\Pi, v'-X\ ^1\Sigma^+, v'')$ emission spectrum from $CO_2^+ + e^-$. $[CO_2]=1.9\times10^{13}$ cm^{-3}. The data have been corrected for the spectral response of the detection system.

which has a branching fraction[41] of 0.16 ± 0.08. The influence of this small contribution to the $CO(a\ ^3\Pi)$ signal is discussed in Sec. IV.

Spectra were obtained over a range of CO_2 concentrations 2×10^{13} to 3.4×10^{14} cm^{-3}. No significant change in the relative intensities of the bands was seen, indicating negligible vibrational relaxation of $CO(a,v')$ by CO_2 under our conditions. The vibrational distribution, $N_{v'}$, in the $CO(a)$ state was determined by analyzing the spectrum in standard fashion

$$I_{v'v''} \propto N_{v'} \cdot q_{v'v''} \cdot \nu^3_{v'v''} \cdot \text{Re}^2_{v'v''}, \tag{10}$$

where $I_{v'v''}$ is the integrated (over wavelength) $v'v''$ band intensity in counts/s/nm, corrected for the spectral response of the detection system, $q_{v'v''}$ is the Franck–Condon factor,[42] $\nu_{v'v''}$ is the transition frequency and Re is the electronic transition moment. All bands in the observed spectrum, excepting those which were very weak, were included in the analysis. Comparison of different bands arising from a given $CO(a,v')$ level indicated a weak dependence of the electronic transition moment on the r centroid of the transition; this effect was included in the analysis. The resulting vibrational distribution for levels $v'=0$ to 3 is $0.49 \pm 0.01 : 0.25 \pm 0.01 : 0.17 \pm 0.01 : 0.10 \pm 0.01$. The population clearly decreases monotonically with increasing vibrational quantum number and can be described by a vibrational temperature of 4200 ± 300 K. Weaker emission was observed from higher vibrational levels of $CO(a)$, as described in Sec. IV C. In the remaining experiments described in this section, the monochromator was set to the peak of the (0,1) $CO(a-X)$ band at approximately 216 nm.

By moving the optical detection assembly along the track, the variation of $CO(a-X)$ emission intensity along the flow tube, for a fixed position of the CO_2 injection point, was recorded. Representative data are shown in Fig. 3 for three

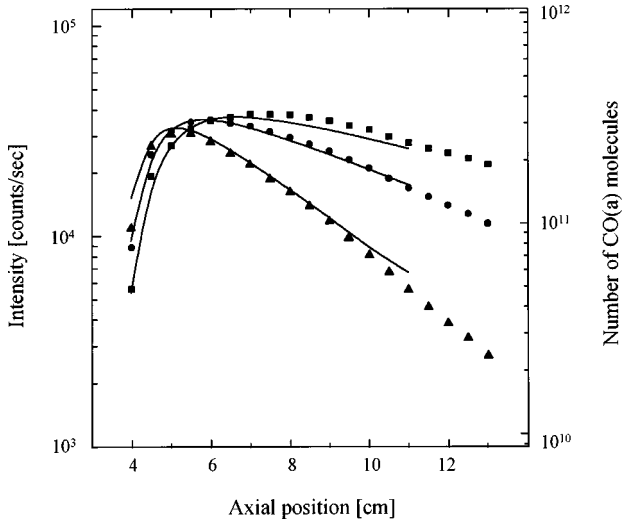

FIG. 3. Dependence of CO($a\ ^3\Pi - X\ ^1\Sigma^+$) (0,1) band intensity on axial position for three CO_2 concentrations. The reagent inlet is at 4 cm. Experimental points: Left-hand scale. $[CO_2]$, cm^{-3}: ■ 1.81×10^{13}; ● 4.83×10^{13}; ▲ 1.30×10^{14}. Solid lines. Right-hand scale. Simulations at $[CO_2]=1.8\times10^{13}$, 5.0×10^{13}, and 1.3×10^{14} cm^{-3}. $k_4=8\times10^{-12}$ $cm^3\ s^{-1}$; $D(CO(a))=450$ $cm^2\ s^{-1}$.

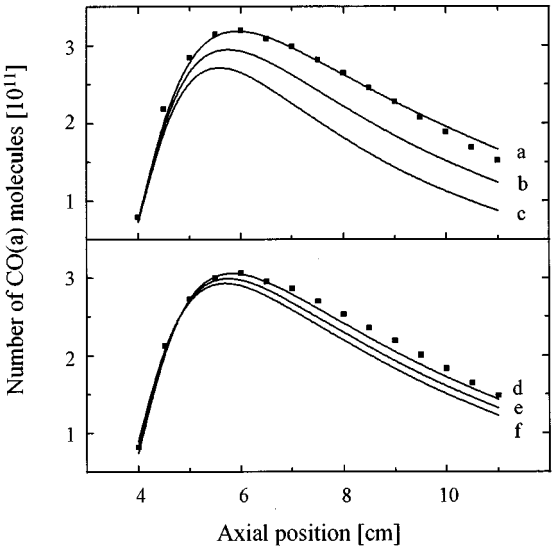

FIG. 4. Simulations of CO($a-X$) emission intensity as a function of axial position. Upper panel. Dependence on quenching rate constant, k_4, with $D(CO(a))=335$ $cm^2\ s^{-1}$. k_4, $cm^3\ s^{-1}$: (a): 8.0×10^{-12}; (b): 1.2×10^{-11}; (c): 1.7×10^{-11}. ■: Experimental points, normalized to the simulations at the maximum of curve (a). Lower panel. Dependence on CO(a) diffusion coefficient, with $k_4=1.0\times10^{-11}$ $cm^3\ s^{-1}$. $D(CO(a))$ $cm^2\ s^{-1}$: (d): 335; (e): 450; (f): 550. ■: Experimental points, normalized to the simulations at the maximum of curve (d).

CO_2 concentrations. The CO_2 is added at the point marked 4 cm. The emission extends far downstream of this point, particularly at low CO_2 concentrations. A small amount of CO_2 diffuses upstream of the injector; the dip in the signal at $z=4$ cm is due to blocking of the light path by the injector loop. As $[CO_2]$ increases, the downstream intensity is reduced, due to quenching of CO(a) by CO_2. The combination of the large radiative lifetime of CO(a) and the electronic quenching means that only about 10% of the CO(a) emits in the observed region of the flow tube.

In order to derive a reliable CO(a) yield, extensive simulations were carried out. Representative fits are included as the solid lines in Fig. 3. These use the values given above for k_1, k_2, and k_3. k_4 was set to 0.8×10^{-11} $cm^3\ s^{-1}$ and the diffusion coefficient of CO(a) (in the He/Ar mix) to our best estimate, $D(CO(a))=450$ $cm^2\ s^{-1}$. For the simulations, the ordinate is the integrated number of CO(a) molecules in a 1 cm disk-shaped slice of the flow tube. The simulations were normalized to the experimental curves at a single point, the maximum in the profile for $[CO_2]=5\times10^{13}$ cm^{-3}. It is seen that the simulations match the dependence of the maximum intensity on $[CO_2]$ and the general shape of the z dependence fairly well, although the simulated curves decay at large z slightly faster than the experimental data. Figure 4 shows the effect of varying $D(CO(a))$ and k_4 in the simulations. As expected, increase in either parameter increases the decay rate at large z. Over the range of CO_2 concentrations used, quenching is a more important loss process than diffusion and thus the z profile depends more strongly on k_4 than on the diffusion coefficient. Figure 4 shows clearly that a value of k_4 of $(0.8$ to $1.0)\times10^{-11}$ $cm^3\ s^{-1}$ yields a much better fit to the data than higher values such as 1.7×10^{-11} $cm^3\ s^{-1}$. From these and other simulations over the whole range of CO_2 concentrations, we deduce a best estimate of k_4 of $(1.0\pm0.2)\times10^{-11}$ $cm^3\ s^{-1}$. Although the variation of k_4 and the diffusion coefficient alters the z profile quite significantly, the effect on the maximum intensity is much smaller, as shown in Fig. 4.

B. $N_2(C-B)$ emission from the reaction of Ar* with N_2

This reaction has been well studied[43,44] and the spectrum is very well characterized.[45] We measured spectra between 280 and 410 nm, including band sequences with $\Delta v=+2$ to -3, involving $N_2(C\ ^3\Pi_u)$ levels with $v'=0-3$. The spectral intensities were analyzed, using the known absolute transition probabilities,[45] to obtain the vibrational distribution in the $N_2(C)$ state: it was found to agree with previous measurements[43] for the $Ar^*(^3P_2)+N_2$ reaction. In the remaining experiments, the monochromator was set to the peak of the (0,0) band at about 337 nm.

For a fixed N_2 injector position, the variation of intensity along the flow tube was measured and is shown in Fig. 5 for N_2 concentrations in the range 1.7×10^{13} to 1.3×10^{14} cm^{-3}. The profile differs from that for CO($a-X$) because the $N_2(C)$ state has a very short radiative lifetime,[45] about 40 ns. The profile thus should parallel that of Ar* concentration and a linear dependence of ln(intensity) versus z is expected. The slight deviation from linearity in Fig. 5, particularly at the highest N_2 concentration, is not fully understood; when the injector was positioned a few centimetres further downstream, improved linearity of the plots was found.

For the absolute calibration of the emission detection system, the total emission signal from N_2^* was used. This involved integration in two distinct dimensions:

(i) Spectral integration over all bands from $v'=0-3$,

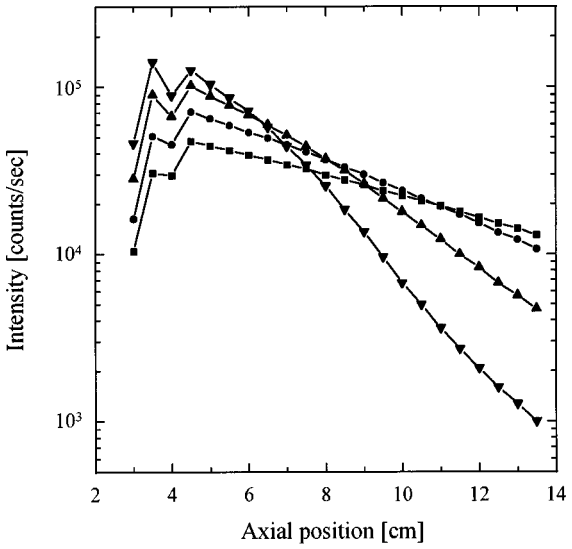

FIG. 5. Dependence of $N_2(C\ ^3\Pi_u - B\ ^3\Pi_g)$ (0,0) band intensity on axial position. The reagent inlet is at 4 cm. The lines are drawn to connect the points. $[N_2]$, cm^{-3}: ■ 1.73×10^{13}; ● 3.08×10^{13}; ▲ 6.21×10^{13}; ▼ 1.35×10^{14}.

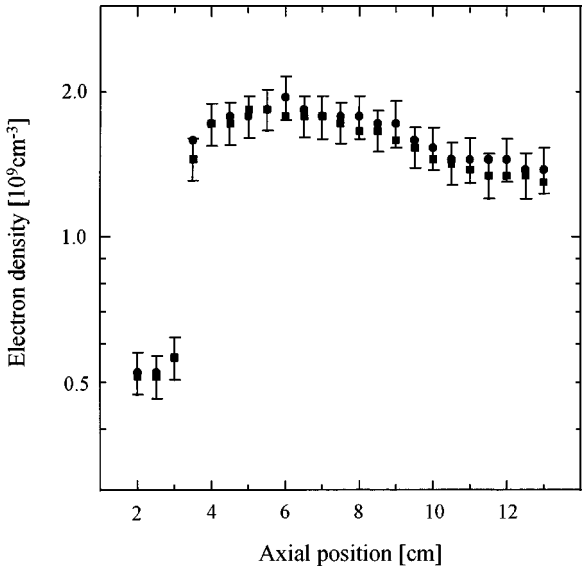

FIG. 6. Langmuir probe measurements of electron density for the reaction $Ar^*(^3P)+NO$. The reagent inlet is at 4 cm. [NO], cm^{-3}: ■ 2.04×10^{14}; ● 3.57×10^{14}.

which was performed using the derived vibrational distribution and the known Einstein emission coefficients.

(ii) Integration of the signal along the flow tube. This involved three steps. First, the signal was integrated over the observed region ($z=3-13$), correcting for the spurious dip which occurs at the injector. Second, by extrapolation, the integration was extended further downstream, assuming exponential decay of the intensity in this region. Third, a small correction was made for competing loss of Ar* atoms, which includes collisional radiative quenching by Ar,[46] diffusion to the wall and quenching by any impurity species. The magnitude of this term was estimated by collecting data such as those in Fig. 5 for various positions of the injector; as the injector was moved downstream, the peak intensity dropped solely due to this competing loss term. The magnitude proved to be slightly larger than that expected for the combined effects of diffusion and quenching by Ar,[47] indicating the presence of small amounts of impurity in the He and/or Ar carrier flows.

The size of the corrections arising from the second and third steps ranged from about 60% of the measured integrated signal at the lowest N_2 concentration to about 7% at the highest concentration. After the corrections had been applied, the integrated signals at the four concentrations in this particular experiment agreed within a 6% range, showing the validity of the analysis procedure.

C. NO^+ production from the reaction of Ar* with NO

When NO was added to a stream of Ar* metastable atoms, a sharp increase in the electron density, as measured by the Langmuir probe, was observed (Fig. 6). The measurements were normally made with the probe positioned on the tube axis. However, close to the injector, where the mixing of the NO with the carrier gas was not complete, the maximum electron density at a given z was located with the probe rotated off axis. The data in Fig. 6 represent the maximum electron density measured at each axial position. The data in all experiments, spanning the range of NO concentrations $1.7-3.5\times10^{14}$ cm^{-3}, showed a small increase in the electron density, n_e, following the jump, with a slow decrease further downstream. As shown by this figure, the observed behavior was independent of NO concentration. Simulations were carried out, which included the loss of NO^+ by dissociative recombination [rate constant $=4.0\times10^{-7}$ $cm^3\ s^{-1}$ (Ref. 48)] and diffusion. The general profile of the experimental data was reproduced, except that the maximum in n_e was predicted to occur closer to the injector. It was concluded that the electron loss processes could be accounted for by adding 10% to the maximum in the electron density profiles in plots such as Fig. 6.

D. Absolute yield of CO(a) in the reaction of CO_2^+ with electrons

Each of the above experiments was repeated until consistent and reproducible relative data were obtained for each experiment. Then, all three reactions were investigated, over a limited range of reagent conditions, in a single experiment to minimize the effect of drifts in conditions. Such experiments were carried out on three separate days.

The Ar*+NO, N_2 data provided an absolute calibration of the emission detection system (at a wavelength of 337 nm) by comparing the Ar* flux (deduced from the NO^+ yield) and the integrated $N_2(C-B)$ emission signal. Use of the spectral response of the detection system extended this absolute calibration to 216 nm, the wavelength at which the $CO(a-X)$ data were collected. The CO(a) simulations essentially yielded the fraction of Ar^+ flux appearing as $CO(a-X)$ emission at the peak in the z profile (Fig. 3);

together with the absolute calibration, this provided a prediction of the signal (counts/s at 216 nm) which would be measured if the yield of $CO(a)$ from $CO_2^+ + e^-$ was unity. Finally, comparison of this predicted signal with the actual measured signal yielded the fraction of CO_2^+ dissociative recombination which produced $CO(a)$. The value obtained from the complete data set was 0.29 ± 0.10, where the stated uncertainty represents one standard deviation and includes the propagated errors from all sources.

IV. DISCUSSION AND CONCLUSIONS

A. Collisional quenching of CO(a) by CO_2

Collisional quenching of $CO(a)$ has been extensively studied.[32] Many polyatomic species, especially those containing hydrogen, quench $CO(a)$ at close to the collision rate. It is accepted that CO_2 is anomalously inefficient, but the rate constant is still uncertain. The present measurement, $(1.0 \pm 0.2) \times 10^{-11}$ cm^3 s^{-1}, is smaller than previous measurements, most of which lie in the range (1.2 to 2.0) $\times 10^{-11}$ cm^3 s^{-1}. It is known that $CO_2^+ + e^-$ recombination contributed to $CO(a)$ production in several of the previous studies. Under those conditions, the present simulations reveal that, at high concentrations of CO_2, the rate of decay of $CO(a)$ does not solely reflect the rate of quenching by CO_2; rather, $CO(a)$ approaches a steady-state condition, at which the decay profile is determined by the rate of formation of $CO(a)$. If this was not taken into consideration in the analysis of the decay data, it would have led to an *underestimation* of the quenching rate constant. Unfortunately, this cannot explain the fact that most of the previous values are larger than the present result.

B. Formation of CO(a) in $CO_2^+ + e^-$ recombination

This study has confirmed the original findings of Wauchop and Broida[17] that a substantial fraction of the recombination of CO_2^+ with e^- passes through the $CO(a\ ^3\Pi)$ state. These authors give no details of the procedure used to extract the absolute yield and thus we prefer the value presented here. It is disconcerting that, as part of their analysis, Wauchop and Broida derived a quenching rate constant for $CO(a) + CO_2$ of 4.1×10^{-11} cm^3 s^{-1}, considerably higher than most other measurements.

Measurements of absolute product yields are subject to several potential sources of error. Those arising from the experimental measurements, the calibration reactions and from the simulations are discussed here. The repeatability of the measurements was good, leading to a random error of less than 10%. The original determination[23] of the NO^+ yield from $Ar^* + NO$ used $Ar^* + N_2 \rightarrow N_2(C)$ as part of the calibration process. It can be deduced that the sizable uncertainty (30%) in the $N_2(C)$ yield fortuitously does not enter into the yield of $CO(a)$ from $CO_2^+ + e^-$. The agreement between the two measurements of the NO^+ yield[23,24] is very good, as discussed by Jones *et al.*[24]

The simulations, which utilize rate constants k_1 to k_4, were also an integral part of our determination of the $CO(a)$ yield. The yield depends directly on the value of k_3. k_2 was fixed within a small range by the need to fit the z dependence of the electron density. Variation of k_1 and k_2 over their expected ranges of uncertainty had a minor effect on the final $CO(a)$ yield. Equivalent fits to the experimental $CO(a-X)$ z profiles could be obtained by simultaneously changing k_4 and the diffusion coefficient of $CO(a)$. Thus these quantities are not determined well, but the maximum $CO(a)$ concentration obtained in the simulations was affected only slightly by these changes. Based on this variation, the limited success in modeling the dependence of the peak $CO(a-X)$ emission intensity on CO_2 concentration and the uncertainty in k_3, we derive an 18% uncertainty in the $CO(a)$ yield arising from the simulations.

Measurements in our flow system have revealed the presence of a small concentration of Ar* metastables, 10%–12% of that of the Ar^+ ions. These react with CO_2 to give $CO(a)$ with a branching fraction[41] of ~ 0.16. Simulations carried out including this reaction led to an 8% contribution to the maximum $CO(a)$ concentration. The derived $CO(a)$ yield of 0.29 presented in the previous section has been corrected for this contribution.

C. Other processes in $CO_2^+ + e^-$ recombination

At present, insufficient information is available to provide a complete picture of energy disposal in $CO_2^+ + e^-$ recombination, even amongst the triplet states of CO. Intense CO emission from the $(a'\ ^3\Sigma^+)$, $(d\ ^3\Delta)$, and $(e\ ^3\Sigma^-)$ states has been observed,[21,40] particularly from $CO(a'$ and $d)$, but no absolute yields have been reported. For $CO(a')$, emission from $v = 3-11$ has been reported, peaking at $v = 5$; for $CO(d)$, $v = 0-6$ are observed, with the peak at $v = 1$.[21,49] At present there appears to be no direct information concerning the populations of levels $v = 0-2$ of the $CO(a')$ state. $CO(a'-a)$ bands from these low-lying levels occur in the ir beyond the spectral detection region of Tsuji *et al.*

Interpretation of the data is complicated by two interesting phenomena. First, cascade emission from $CO(a'$, d, and $e)$ contributes to the population of the $CO(a)$ state. Using the reported vibrational distributions and relative populations in these two states, the relative vibrational distribution in the $CO(a, v = 0-3)$ levels arising from the $(a'-a)$ and $(d-a)$ transitions was calculated and found to be comparable to that observed in the present study. It is possible therefore that cascade emission contributes significantly to the observed $CO(a)$ population.

Second, these triplet states are connected also by collisional crossing between $CO(a, v \geq 4)$ and the $CO(a')$ state and between $CO(a, v \geq 8)$ and the $CO(d)$ state (see Fig. 1). Ottinger *et al.*[50] have studied $CO(a')$ emission resulting from collisions of He with a beam of $CO(a)$ molecules with a vibrational temperature of about 6400 K and find a vibrational distribution in the a' state which is comparable to that reported by Tsuji *et al.*[21] We have obtained preliminary evidence for the occurrence of $CO(a \rightarrow a')$ collision-induced transitions in the CO_2^+ recombination system by detection of weak emission from $CO(a, v = 4-7)$ [which have similar

energies to CO(a',$v=0-4$)]. These emissions decay down the flow tube significantly more rapidly than CO(a,$v=0-3$), as expected if an additional loss process is available. Under the experimental conditions of the present study and of that of Tsuji *et al.*, CO($a\rightarrow a'$) and, where energetically possible, CO($a\rightarrow d$) collision-induced transfer is expected to be a major loss process for CO(a,$v\geqslant 4$), while the reverse processes are expected to be less dominant because of the lower radiative lifetimes of the CO(a') and CO(d) states. We conclude that it is possible that CO($a\rightarrow a'$) transitions contribute to the observed CO(a') [and CO(d)] emissions in $CO_2^+ + e^-$ recombination under flow tube conditions. Further studies are planned to clarify the pathways leading to formation of the CO triplet states in this reaction system.

Our results, combined with those of Gutchek and Zipf,[16] show that about one-third of $CO_2^+ + e^-$ recombination events form singlet and triplet excited states of CO. We expect that the remainder gives rise to CO($X\ ^1\Sigma^+$)+O(^3P,^1D,^1S) products. Recombination occurs by capture of an electron to form a repulsive electronic state of CO_2, possibly via an intermediate bound Rydberg state. Potential-energy surfaces of CO_2 are not known sufficiently well for the exact path or paths to be determined.[51,52] Also, because of the very large number of electronic states of CO_2 which correlate with CO($a\ ^3\Pi$, $a'\ ^3\Sigma^+$, and $d\ ^3\Delta$)+O(^3P), it is difficult to predict which state or states are involved.

It is interesting, however, to compare the dissociation pathways from $CO_2^+ + e^-$ recombination with those from photodissociation of CO_2. In separate studies, the absorption coefficient of CO_2 up to (and beyond) the first ionization limit[53] and the cross sections for photodissociation to CO($a\ ^3\Pi$),[54] CO($a'\ ^3\Sigma^+$ and $d\ ^3\Delta$),[55] and CO($A\ ^1\Pi$) (Ref. 56) have been measured. For photoexcitation at 90.0 nm, close to the ionization energy, the results agree qualitatively with those for $CO_2^+ + e^-$ recombination. First, the measured yield of CO(a) from CO_2 photodissociation is about 60%, compared to about 30% from CO_2^+ recombination. As in our experiments, this figure includes formation via cascade from higher-energy triplet states. Second, CO($a'\ ^3\Sigma^+$) and CO($d\ ^3\Delta$) are important products but their yield at 90.0 nm appears to be somewhat smaller than that of CO(a). Finally, the vibrational distributions in CO(a, a', and d) are similar to those resulting from CO_2^+ recombination. One possible reason for this similarity in behavior is that both $CO_2(X)$ and $CO_2^+(X)$ are linear molecules and have very similar bond lengths. Thus similar regions of the potential energy surfaces will be accessed initially in the two processes.

It cannot, however, be assumed that identical excited states of CO_2 are involved in photodissociation and CO_2^+ recombination, because of the specific selection rules for the former process. The absorption and photodissociation spectra are highly structured, showing that several electronic states contribute to each dissociation channel. It would be interesting to compare the CO_2^+ recombination products with those from $HCO^+ + e^-$, because far fewer valence excited states are expected to be accessible in this latter system.

ACKNOWLEDGMENTS

This work was supported in part by NASA under Grant No. NAGW 1764. Theodosia Gougousi is grateful to the Andrew Mellon Foundation for providing a predoctoral fellowship.

[1] G. C. Reid, Adv. At. Mol. Phys. **63**, 375 (1976).
[2] J. B. Lauderslager, *Kinetics of Ion Molecule Reactions* (Plenum, New York, 1979), p. 405.
[3] G. Turban, Pure Appl. Chem. **56**, 215 (1984).
[4] J. L. Fox and A. Dalgarno, J. Geophys. Res. **84**, 7315 (1979).
[5] J. L. Fox and A. Dalgarno, J. Geophys. Res. **86**, 629 (1981).
[6] S. L. Guberman, Nature (London) **327**, 408 (1987).
[7] D. Talbi, F. Pauzat, and Y. Ellinger, Chem. Phys. **126**, 291 (1988).
[8] D. R. Bates, Astrophys. J. **306**, L45 (1986).
[9] N. G. Adams, C. R. Herd, M. Geoghegan, D. Smith, A. Canosa, J. C. Gomet, B. R. Rowe, J. L. Queffelec, and M. Morlais, J. Chem. Phys. **94**, 4852 (1991).
[10] T. Gougousi, R. Johnsen, and M. F. Golde, J. Chem. Phys. **107**, 2430 (1997).
[11] M. Tsuji, K. Kobarai, H. Kouno, H. Obase, and Y. Nishimura, J. Chem. Phys. **94**, 1127 (1991).
[12] N. G. Adams and L. M. Babcock, J. Phys. Chem. **98**, 4564 (1994).
[13] S. Datz, G. Sundström, Ch. Biedermann, L. Broström, H. Danared, S. Mannervik, J. R. Mowat, and M. Larsson, Phys. Rev. Lett. **74**, 896 (1995).
[14] D. Kella, L. Vejby-Christensen, P. J. Johnson, H. B. Pedersen, and L. H. Andersen, Science **276**, 1530 (1997).
[15] G. Herzberg, T. J. Hugo, S. G. Tilford, and J. D. Simmons, Can. J. Phys. **48**, 3004 (1970).
[16] R. A. Gutchek and E. C. Zipf, J. Geophys. Res. **78**, 5429 (1973).
[17] T. S. Wauchop and H. P. Broida, J. Chem. Phys. **56**, 330 (1972).
[18] G. Taieb and H. P. Broida, Chem. Phys. **21**, 313 (1977).
[19] G. M. Lawrence, Chem. Phys. Lett. **9**, 575 (1971).
[20] F. R. Burden, M. A. A. Clyne, and A. Fontijn, Chem. Phys. **65**, 123 (1982).
[21] M. Tsuji, M. Nakamura, Y. Nishimura, and H. Obase, J. Chem. Phys. **103**, 1413 (1995).
[22] H. Hotop and A. Niehaus, Int. J. Mass Spectrom. Ion Phys. **5**, 415 (1970).
[23] M. F. Golde, Y.-S. Ho, and H. Ogura, J. Chem. Phys. **76**, 3535 (1982).
[24] M. T. Jones, T. D. Dreiling, D. W. Setser, and R. N. McDonald, J. Phys. Chem. **89**, 4501 (1985). The authors have reanalyzed their data to give an NO^+ yield of 0.34 ± 0.15.
[25] J. H. Kolts, H. C. Brashears, and D. W. Setser, J. Chem. Phys. **67**, 2931 (1977).
[26] N. Sadeghi and D. W. Setser, Chem. Phys. Lett. **82**, 44 (1981).
[27] R. Johnsen, E. V. Shun'ko, T. Gougousi, and M. F. Golde, Phys. Rev. E **50**, 3994 (1994).
[28] R. Shul, B. L. Upschulte, R. Passarella, R. G. Keesee, and A. W. Castleman, J. Phys. Chem. **91**, 2556 (1987).
[29] F. C. Fehsenfeld, E. E. Ferguson, and A. L. Schmeltekopf, J. Chem. Phys. **45**, 404 (1966).
[30] T. Gougousi, M. F. Golde, and R. Johnsen, Chem. Phys. Lett. **265**, 399 (1997).
[31] M. Geoghegan, N. G. Adams, and D. Smith, J. Phys. B **24**, 2589 (1991).
[32] K. Schofield, J. Phys. Chem. Ref. Data **8**, 723 (1979).
[33] W. Lindinger and D. Albritton, J. Chem. Phys. **62**, 3517 (1975).
[34] *Handbook of Chemistry and Physics*, 74th ed. (CRC, Boca Raton, 1993).
[35] W. G. Clark and D. W. Setser, Chem. Phys. Lett. **33**, 71 (1975).
[36] D. Levron and A. V. Phelps, J. Chem. Phys. **69**, 2260 (1978).
[37] C.-J. Hwang, R. C. Jiang, and T.-M. Su, J. Chem. Phys. **84**, 5095 (1986).
[38] C. B. Collins and W. W. Robertson, J. Chem. Phys. **40**, 701 (1964).
[39] D. Smith, N. G. Adams, and E. Alge, J. Phys. B **17**, 461 (1984).
[40] M. Skrzypkowski, R. Johnsen, and M. F. Golde (unpublished results).
[41] J. Balamuta and M. F. Golde, J. Chem. Phys. **76**, 2430 (1982).
[42] D. Albritton (private communication).
[43] T. D. Nguyen and N. Sadeghi, Chem. Phys. **79**, 41 (1983).
[44] D. W. Setser, D. H. Stedman, and J. A. Coxon, J. Chem. Phys. **53**, 1004 (1970).
[45] A. Lofthus and P. H. Krupenie, J. Phys. Chem. Ref. Data **6**, 113 (1977).
[46] M. F. Golde, in *Gas Kinetics and Energy Transfer, Specialist Periodical Reports*, edited by P. G. Ashmore and R. J. Donovan (Chemical Society, London, 1976), Vol. 2, p. 121.

[47] J. H. Kolts and D. W. Setser, J. Chem. Phys. **68**, 4848 (1978).
[48] R. Johnsen, Int. J. Mass Spectrom. Ion Processes **81**, 67 (1987).
[49] M. Tsuji (private communication).
[50] Ch. Ottinger, A. F. Vilesov, and D. D. Xu, J. Phys. Chem. **99**, 15642 (1995).
[51] P. J. Knowles, P. Rosmus, and H.-J. Werner, Chem. Phys. Lett. **146**, 230 (1988).
[52] A. Spielfiedel, N. Feautrier, G. Chambaud, P. Rosmus, and H.-J. Werner, Chem. Phys. Lett. **183**, 16 (1991).
[53] R. C. Nakata, K. Watanabe, and F. M. Matsunaga, Sci. Light **14**, 54 (1965).
[54] G. M. Lawrence, J. Chem. Phys. **56**, 3435 (1972).
[55] D. L. Judge and L. C. Lee, J. Chem. Phys. **58**, 104 (1973).
[56] E. P. Gentieu and J. E. Mentall, J. Chem. Phys. **58**, 4803 (1973).